Journal of Materials Chemistry A

Accepted Manuscript

This article can be cited before page numbers have been issued, to do this please use: W. Wang, S. Sun, Q. An, L. Zhang, J. Liu and W. A. Goddard, III, *J. Mater. Chem. A*, 2016, DOI: 10.1039/C6TA09275F.

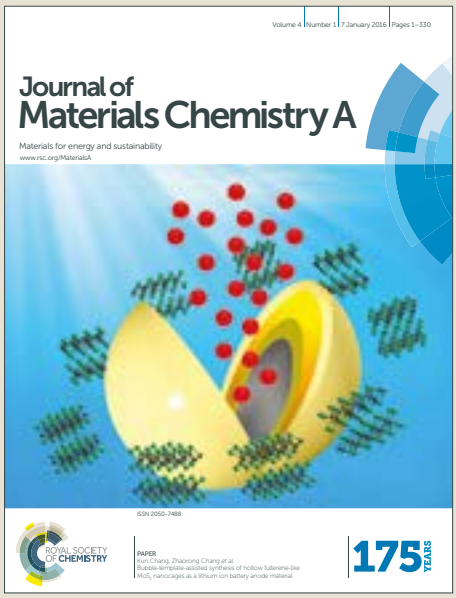

ROYAL SOCIETY OF CHEMISTRY

rsc.li/materials-a

Efficient Photocatalytic Reduction of Dinitrogen to Ammonia on Bismuth Monoxide Quantum Dots

Songmei Sun[1], Qi An[2], Wenzhong Wang[1]*, Ling Zhang[1], Jianjun Liu[1]*, William A. Goddard III[2]

[1]State Key Laboratory of High Performance Ceramics and Superfine Microstructure, Shanghai Institute of Ceramics, Chinese Academy of Sciences, Shanghai 200050, P. R. China

[2]Division of Chemistry and Chemical Engineering, California Institute of Technology, Pasadena, California 91125, United States

*Address correspondence to wzwang@mail.sic.ac.cn, jliu@mail.sic.ac.cn

Abstract

N_2 reduction to ammonia by solar light represents a green and sustainable ammonia synthesis approach which helps to suppress the global warming and energy crisis. However, conventional semiconductors usually suffer from low activity or poor stability, largely suppressing the application of this technology. Here, we report bismuth monoxide (BiO) quantum dots with an average size of 2-5 nm exhibited efficient photocatalytic activity for ammonia synthesis under simulated solar light. A highly efficient ammonia synthesis rate of 1226 μmol/g·h is achieved without the assistant of any sacrificial agent or co-catalyst, which is about 1000 times higher than that of traditional Fe-TiO_2 photocatalyst. Kinetic analysis reveals that cooperation of three low valence surface Bi (II) species markedly enhances N_2 activation by electron donation, which finally resulted in the highly efficient N_2 photoreduction performance. This work will shed light on designing efficient and robust N_2 reduction photocatalysts.

View Article Online
DOI: 10.1039/C6TA09275F

Introduction

The reduction of dinitrogen (N_2) to ammonia is a requisite transformation for the life growth and survival.[1-4] Although over 78% of the atmosphere is composed of dinitrogen molecules, they are not used by most of organisms due to strong N≡N bond, nonpolarity and high ionization potential.[5,6] At present, most of the required nitrogen for human beings is still originated from the energy-intensive Haber–Bosch ammonia synthesis process,[7,8] which consumes 1-2% of the world's energy supply and generating more than 300 million tons of carbon dioxide annually.[9-12] In contrast, dinitrogen photoreduction to ammonia by solar light represents a green and sustainable ammonia synthesis route without fossil fuel consumption and CO_2 emissions.[13-16] However, the state-of-the-art efficiencies for ammonia synthesis by this approach are still far away from the industrial demand.[17-24]

Generally, the rate-determining step for N_2 reduction is cleavage of the N≡N bond.[5,6] N_2 activation by electron donation from some reducing active sites are indispensable for the promotion of N≡N bond cleavage,[25] but such reducing active sites are rarely existed on most of the semiconductor photocatalysts. Up to the present, the majority of the reported N_2 photoreduction catalysts are only have defect type activation centers,[17-24] which resulted in the unsatisfied photocatalytic performance because of their limited defect concentrations. Besides, defect states often suffer from thermal instability and increased charge carrier recombination, further prevents their practical application for artificial ammonia synthesis. Consequently, developing an ideal photocatalytic material which has high concentration of non-defect type activation centers with robust stability holds the key to achieving a breakthrough in N_2 photoreduction technology.

Using low valence metal species in low-valent metal oxide semiconductors for N_2

View Article Online
DOI: 10.1039/C6TA09275F

activation may be a viable strategy to achieve this important goal. Low-valent metals in semiconductor solids have fewer coordination atoms than those in their high-valent state and are hence chemically unsaturated to facilitate molecules chemisorption.[26] Owing to the strong electron donation power, low-valent metal species such as Fe, Mo, Zr, Ti *etc.*, have been widely studied for N_2 activation in organometallic complexes,[9,16,27-30] although a stoichiometric excess of strong reducing agents (such as Na, K) and extra proton sources are generally required to further generate NH_3 in these reaction systems. Different from organometallic complexes, low-valent metal species in semiconductor material may act as both the N_2 activation and hydrogenation centers without an extra reducing agents, which allows quick reaction kinetics for N_2 reduction, because the conduction band of a metal oxide semiconductor was usually hybridized by the metal p, d orbitals,[31] and photogenerated electrons were mainly located on the metal sites. Moreover, different from defect-type active sites, lattice low-valent metal species can refrain from becoming an electron-hole recombination center and all of the surface low-valent metal sites could contribute to the catalysis reactions theoretically. In these regards, low-valent metal oxide semiconductors are expected to exhibit high photocatalytic activity for N_2 photoreduction. To confirm this opinion, herein low valent bismuth monoxide (BiO) was selected as an ideal model material to study the N_2 photoreduction performance. We focus on low valent bismuth (II) because it has high electron donation power and empty 6d orbitals for N_2 adsorption and activation. More importantly, bismuth based materials have been widely studied with various catalytic applications.[32-34]

Experimental

Preparation of BiO. Firstly, sodium oleate (2.2 mmol) and $Bi(NO_3)_3 \cdot 5H_2O$ (0.4

mmol) were successively added to distilled water (20 mL). After vigorous stirring for 2 h, 20 mL water was added and the suspension was then transferred to a 50 mL Teflon-lined autoclave, sealed and heated at 140 ºC for 17 h. The system was then allowed to cool down to room temperature. The obtained solid products were collected by centrifugation, washed with absolute ethanol three times, and then freeze-dried for further characterization. For comparison, 0.2wt % Fe-doped TiO_2 was prepared according to a previous report by coprecipiation and calcination process at 500 ºC for 3h[18]. The XRD pattern of the Fe-doped TiO_2 was shown in Fig. S1.

Characterization. The purity and the crystallinity of the as-prepared samples were characterized by powder X-ray diffraction (XRD) on a Japan Rigaku Rotaflex diffractometer using Cu Kα radiation while the voltage and electric current were held at 40 kV and 100 mA. The transmission electron microscope (TEM) analyses were performed by a JEOL JEM-2100F field emission electron microscope. X-ray photoelectron spectroscopy (XPS) was carried out by irradiating the sample with a 320 μm diameter spot of monochromated aluminum Kα X-rays at 1486.6 eV under ultrahigh vacuum conditions (performed on ESCALAB 250, Thermo Scientific Ltd.). UV–vis diffuse reflectance spectrum (DRS) of the sample was measured using a Hitachi UV-3010PC UV–vis spectrophotometer. Fourier transform infrared (FTIR) spectrum of concentrated ammonia product was performed with a spectrophotometer (Nicolet 380, Thermo, USA). Nitrogen temperature-programmed desorption (N_2-TPD) measurements were performed on a ChemiSorb 2750 instrument. Typically, 20 mg of the sample, placed in a glass tube, was pretreated by a He gas flow at 150 °C for 2 h, and then cooled down to 50 °C. The adsorption of N_2 was performed in a 99.999% N_2 gas flow for 2 h at 50°C. After purge by He gas, the sample was heated from 50 °C to 450 °C at a rate of 10 °C/min. The TPD signal was recorded by a thermal conductivity

View Article Online
DOI: 10.1039/C6TA09275F

detector. All of the gas flow rates were set as 30 mL/min. ^{1}H NMR spectra were acquired on a Bruker AV500 NMR spectrometer.

Photocatalytic Test. Photocatalytic N_2 reduction were performed under a 500 W Xe lamp located approximately 10 cm from the sample. The reaction cell (capacity 600 mL) was made of Pyrex glass with a quartz window on top. For the atmospheric N_2 fixation, 0.05 g of the as-prepared photocatalyst powder was dispersed in 200 mL deionized water and then stirring under the simulated solar light irradiation. For ^{15}N isotopic labelling experiment, the reaction cell was enclosed by a quartz window on top. N_2 (50% $^{15}N_2$, 50% $^{14}N_2$) gas was slowly bubbled through the reaction vessel, which contained 200 mL deionized water until that was saturated. Then the reaction vessel was sealed and irradiated under the simulated solar light irradiation. During the photocatalytic tests, the temperature of the reaction vessel was maintained at 25 ºC by providing a flow of cooling water. The concentration of ammonia in the reactor solution was measured using the indophenol blue method. The amount of evolved O_2 was determined by using online gas chromatography.

Computational Methods. Periodic density functional theory (DFT) calculations with spin-polarization were performed using the VASP code. The non-local exchange and correlation energies were described using a generalized gradient approximation with the Perdew–Burke–Ernzerhof (PBE) functional (PBE-GGA). The electron-ion interactions were described by projector augmented wave (PAW) potential. The plane wave-plane basis set with energy cutoff of 400 eV and 4×4×4 k-point Monkhorst-Pack grid were used in our calculations. The convergence criterions for electronic SCF and force were set as less than 1.0×10^{-6} eV and 0.01 eV/Å, respectively.

Electrochemical measurements. Electrochemical measurements were performed on

View Article Online
DOI: 10.1039/C6TA09275F

a CHI 660D electrochemical workstation (Shanghai Chenhua, China) using a standard three-electrode cell with a working electrode, a platinum wire as counter electrode, and a standard saturated calomel electrode (SCE) in saturated KCl as reference electrode. The working electrodes were prepared by dip-coating: Briefly, 5 mg of photocatalyst was suspended in 0.1 mL of ethanol in the presence of 1% Nafion to produce slurry, which was then dipcoated onto a 2 cm × 1.5 cm FTO glass electrode and drying at 25 °C.

Calculation of electron transfer number: For an adsorption-controlled and irreversible electrode process, according to Laviron,[35] Ep is defined by the following equation:

$$Ep = E^0 + (RT/anF)\ln(RTK^0/anF) + (RT/anF)\ln v$$

where R is molar gas constant, T is thermodynamic temperature, F is faraday constant, a is transfer coefficient, k^0 is standard rate constant of the reaction, n is electron transfer number involved in the rate-determining step, ν is scan rate(mV/S), and E^0 is formal potential. For an irreversible electrode process, a≈0.5.

Results and Discussion

We designed an oleate-modified hydrothermal synthesis method to obtain the desired BiO material. Oleate ions played an important role in the formation of this low-valence bismuth oxide compound, as shown in Fig. 1. Initially each Bi^{3+} ion interacts electrostatically with three oleate ions to form Bi-oleate complexes, which then aggregated into larger Bi-oleate particles driven by the hydrophobic effect of the oleate tails. The presented extra oleate ions in the solution accumulated around the Bi-oleate complex by hydrophobic carbon tails to form stable Bi-oleate micelles with hydrophilic outer shell which dispersed homogeneously in the reaction solution. The

View Article Online
DOI: 10.1039/C6TA09275F

BiO compound was nucleated through a dehydration and condensation reaction after permeation of a small amount of OH^- into the Bi-oleate micelles. This process was hindered by the strong steric effect from oleate which has long aliphatic carbon chain to prevent polar ions to entry. Since the reductivity of unsaturated carbon–carbon double bonds in oleate, the Bi (III) was gradually reduced to Bi (II) during reaction with OH^- to form low-valence BiO compound in the micelles. Without the addition of oleate ions, Bi_2O_3 is the final hydrothermally synthesized product. The as-prepared BiO compound exhibited quantum sized spherical-like morphology (quantum dots) with average size of 2-5 nm (Fig. 2a). A high magnified TEM image (Fig. 2b) gives more details of the microstructure, which revealed the single crystal nature of the BiO particles. From a high resolution TEM (HRTEM) image in Fig. 2c, (003) and (100) planes of BiO (space group R3m) with a d spacing of 0.325 and 0.336 nm were clearly observed, which belong to the [010] zone axis of BiO. The schematic crystal structure of BiO along the [010] direction (Fig. 2d) displayed the same orientation and arrangement of (003) and (100) planes as that observed from Fig. 2c. The purity and crystallinity of the BiO particles were investigated by X-ray diffraction pattern. As shown in Fig. 2e, all of the diffraction peaks can be indexed to the hexagonal phase of BiO (JCPDS No.27-0054). No other likely impurities, such as Bi_2O_3 or $Bi(OH)_3$, were detected. The broad diffraction peaks were ascribed to its quantum size which is calculated to be about 3 nm in average based on the Scherrer equation. XPS spectrum further confirmed this low-valent bismuth (II) monoxide compound. As shown in Fig. 2f, the binding energies of Bi $4f_{5/2}$ and Bi $4f_{7/2}$ peaks in original BiO surface mainly located at 164.55 eV and 159.26 eV which is originated from the residual surface-adsorbed Bi (III)-oleate precursor. However, in the case of an etched surface, the binding energies of the Bi $4f_{5/2}$ and Bi $4f_{7/2}$ peaks mainly decreased to 162.35 eV

View Article Online
DOI: 10.1039/C6TA09275F

and 156.95 eV, proving the existence of low-valent bismuth species in a cleaner BiO surface. Optical absorption property of the prepared BiO was investigated by UV–vis diffuse reflectance spectroscopy which exhibited an intense UV-vis light absorption at wavelengths shorter than 430 nm (Fig. S2), indicating a band gap of 2.88 eV for the BiO sample.

To study the photocatalytic N_2 reduction property of the BiO catalyst, 0.05 g of the BiO particles was dispersed in 200 mL of deionized water and then subsequently irradiated under simulated solar light irradiation. Control experiments showed that NH_4^+ cannot be generated in the absence of BiO catalyst or solar light irradiation. In contrast, simulated solar light irradiation resulted in continuous ammonia generation by the BiO sample (Fig. 3a). After 24 h of irradiation, the BiO catalyst generated 7.4 mg/L of NH_4^+ from pure water in air. In an acidic reaction solution (pH 3.8) which could provide excess protons to decrease the kinetic barrier for N_2 reduction, the generated ammonia concentration by the BiO catalyst was increased to 20.6 mg/L within 24 h, with an much improved ammonia synthesis rate of about 1226 μmol/g (catalyst)·h, 1000 times higher than that of traditional Fe-TiO_2 photocatalyst (Fig. 3a) under the same conditions. When the reaction was performed in 15% aqueous methanol, a known sacrificial electron donor, the ammonia synthesis rate was further significantly improved, producing a total NH_4^+ amount of 0.7 mmol after 24 h (Fig. 3b), equivalent to a turnover number of 3.18. This suggests that ammonia evolution under these conditions is catalytic. The increase in the ammonia synthesis rate in aqueous methanol indicates the BiO quantum dots are able to photooxidize methanol. Under the same conditions, no ammonia generation was detected with the BiO catalyst both in pure water and aqueous methanol in argon saturated solution, indicating the ammonia in the reaction system was originated from N_2 reduction. The

View Article Online
DOI: 10.1039/C6TA09275F

stability of the BiO catalyst under acid conditions is also investigated. After 5 consecutive runs (120 h) for N_2 reduction, the photocatalytic performance of the BiO particles was well-maintained (Fig. 3c). The TEM image of the BiO catalyst after the cycle of reaction also indicates the stability of the BiO catalyst (Fig. S3).

To further confirm the detected NH_4^+ in our experiment was indeed originated from N_2 reduction, we performed an isotopic labelling study using 50 vol % $^{15}N_2$ as the purge gas. Infrared spectroscopy was used to characterize the NH_4^+ product. The IR spectra (Fig. 3d) indicate that both the $^{15}NH_4^+$ and $^{14}NH_4^+$ exist in the reaction solution when using the 50% $^{15}N_2$ labelled N_2, while only $^{14}NH_4^+$ is detected when using pure $^{14}N_2$. The infrared absorption peak of $^{14}NH_4^+$ was located around 1405 cm^{-1}, while the peak position for $^{15}NH_4^+$ is at 1358 cm^{-1} which is in good agreement with the value estimated according to the isotope effect (that is, 1405 $cm^{-1}\times(14/15)^{1/2}$=1357 cm^{-1})[25]. The isotope labelling study further proved that the NH_4^+ originates from the photocatalytic N_2 reduction process. ^1H NMR spectrum was also used for detecting the $^{15}NH_4^+$ specie in the obtained ammonia product. As shown in Fig. S4, both of $^{15}NH_4^+$ and $^{14}NH_4^+$ were observed in the NMR spectrum. The molar ratio of the $^{15}NH_4^+$ to $^{14}NH_4^+$ was about 2.7 : 3, which is close to the initial $^{15}N_2$ content.

It is of significant importance to understand the underlying mechanism on the high photocatalytic activity of BiO in reducing N_2 in order to develop other efficient photocatalysts. Quantum chemical calculations based on density functional theory (DFT) were conducted to investigate the possible N_2 activation and hydrogenation process on BiO catalyst. According to the experimental observation from HRTEM image, a presentative BiO {010} surface was selected to investigate the N_2 activation and hydrogenation performance. First, partial charge density nearby Fermi level was calculated to analyze the possible interaction positions of BiO surfaces with N_2. As

shown in Fig. 4a and 4b, the valence bands of BiO near Fermi levels are mainly generated by p-electrons of Bi atoms. The charge distribution on BiO {010} surface is significantly localized and accumulated around Bi atoms, which indicated that N_2 activation by electron donation may take place upon the Bi activation centers. The extent of N_2 activation and hydrogenation on the BiO surface can be reflected by the change of $N-N$ bond length. Fig. 4c presents N-N bond distance evolutions with adding hydrogen atoms on the BiO {010} surfaces. For comparison, the corresponding evolutions without catalyst are also plotted. As shown in Fig. 4c, the BiO {010} surface has high catalytic activity on activation of N≡N bond in N_2H_n (n=0-3). The N-N bond length could be elongated from 1.09 Å to 1.12Å when it is near the BiO {010} surface. The N-N bond length could be further increased along with hydrogenation until three H atoms were hydrogenated, indicating that N≡N bond may be broken after three H atoms were added by the BiO catalyst. Considering the N_2 photoreduction experiment was performed in water in this study, the influence of water molecules on the N_2 activation and hydrogenation was also investigated. The calculated result indicates the catalytic activity of BiO was not changed with adding H_2O on surface. In addition, H_2O molecules covering on surface can quickly dissociate into H^+ and OH^-, providing enough hydrogen for ammonia generation. Besides, the binding energy calculations reveal a weaker interaction between N_2H_n and water-covered BiO surface than that in dry surface (Fig. 4d). This indicates that water on the BiO {010} surface is advantageous to improve N_2 photoreduction performance since hydrogenated N_2H_n is easy to be desorbed from catalyst. Temperature programmed desorption (TPD) investigation was also conducted to visualize the adsorption and activation of N_2 on the surface of the BiO catalyst. As shown in Fig. S5, two peaks at 295 ºC and 330 ºC were clearly observed for N_2

View Article Online
DOI: 10.1039/C6TA09275F

desorption, which indicated the excellent N_2 chemisorption on BiO catalyst.

Photoelectrochemical measurements further revealed the possible reasons for the high performance of BiO catalyst. As shown in Fig. 5a, two well-defined cathodic peaks around –0.7 V and -1.2 V appears in the cyclic voltammetry in N_2 saturated 0.5 M Na_2SO_4 solution for BiO electrode in an acid solution (pH=3.8). The pH value of the electrolyte was adjusted by dilute H_2SO_4. The lower reduction peak around -0.7 V only arises after the electro-reduction process proceeding a certain time (Fig. 5a and Fig. S6), indicating this reduction peak may be originated from further reduction of intermediates during the photoelectrochemical process. Therefore the N_2 reduction peak around -1.2V (E_p) was adopted for the kinetic study under acid conditions. As shown in Fig. 5a, the peak current densities increased with increasing the scan rates (ν). The number of electron transfer (n) involved in the N_2 reduction can be calculated from the slope of the E_p-lnν (ESI). The value of n was calculated to be 2.93 at the potential 20-100 mV, indicating a one-step three electron transfer N_2 reduction process may be existed on the BiO surface. As is well known, nitrogen fixation is a proton-coupled reaction.[36] Although the BiO surface could provide enough low valent Bi (II) activation centers, excess H^+ is important to realize a proton coupled multi-electron reduction process. In a neutral reaction solution, the electron transfer number was decreased to 1.34 based on the analysis of the reduction peak around -0.9 V (Fig. 5b), indicating N_2 reduction on BiO catalyst in neutral solution may be realized by six consecutive one-electron redox step, resulting in a much lower ammonia synthesis rate. This is in line with the lower photocatalytic N_2 reduction activity of BiO at pH=7. Besides, a decreased cathodic current density (Fig. 5c) in N_2-saturated reaction system was observed when compared with that in air saturated solution, which proved the larger amount of electrons transfer from the BiO catalyst

to the N_2 molecule in N_2-saturated reaction system under the same conditions. Fig. 5d is Mott−Schottky spectrum of the BiO sample, which is usually used for the analysis of the flat band potential (E_{fb}) of semiconductor electrodes.[37] The positive slope of the plot indicates the BiO catalyst is n-type semiconductor with electrons as the majority charge carriers. The E_{fb} value which was calculated from the intercept of the axis with potential value was at −0.69 V *vs* SCE. For many n-type semiconductors, E_{fb} is considered to be about 0.1 V below the conduction band (E_{cb}).[38] Based on this, the estimated E_{cb} values of the BiO sample was -0.55 V *vs.* NHE. According to the thermodynamic data of N_2H_3 reported by Bauer,[39] the N_2 reduction potential via $N_2 + 3H^+ + 3e^- \rightarrow N_2H_3$ is not larger than −0.485 V *vs.* NHE. This indicates the photogenerated electrons in the BiO catalyst could energetically reduce the N_2 molecular via a proton-coupled three-electron reduction process. Besides, the valence band potential of the BiO catalyst which estimated from the band gap and E_{cb} was also energetically large enough (2.39 V *vs.* NHE) for water oxidation (1.23 V *vs.* NHE) under acid condition, indicating water could efficiently act as the sacrificial electron donor for ammonia generation. All of these studies proved the possibility of highly efficient one-step three-electron N_2 reduction on BiO catalyst, which may be realized by cooperation of three adjacent low valent Bi (II) activation centers. This process is difficult to occur in traditional N_2 reduction photocatalyst which only has isolated defect-type activation centers.

The crystal structure and the coordination environment of BiO compound may play an important role for its highly efficient photocatalytic N_2 reduction performance. As shown in Fig. 2d, the BiO compound exhibits a hexagonal tunnel structure along the [010] direction, which built up from three alternately arranged Bi groups and O groups. The entrance diameter of this tunnel structure is about 4.4～4.7 Å, large

View Article Online
DOI: 10.1039/C6TA09275F

enough for structurally filling one N_2 molecular (diameter 3 Å). A careful observation for local structure of BiO indicates BiO_4 presents pyramidal unit with two ∠OBiO angles of 114.2° and 104.2°, far away from tetrahedral structure (Fig. S7). This indicates that bismuth atoms may take an orbital hybridization of sp^3d to form orbital distribution of trigonal biyramid, leaving a lone pair of electrons in the Bi atom. The N_2 molecule may be stretched and activated by three alternatively arranged Bi atoms through donating electrons to the empty 6d orbitals of Bi atom and accepting electrons from the lone pairs of Bi atom to its three unoccupied anti-bonding orbitals (π^*2p_y, π^*2p_z and σ^*2p_x), resulting in a $1N_2$-3Bi side-on bond structure (Fig. 6a). The electron donations from ajacent three low valence bismuth ions will strongly weaken the N≡N bond, which facilitates a one-step three electron N_2 reduction process in a successive photocatalytic process by proton and electron transfer (Fig. 6b).

Based on the above analysis, the possible N_2 reduction reactions on BiO surface under acid conditions were proposed as following.

$$BiO + hv \longrightarrow BiO(h^+ + e^-) \quad (1)$$

$$N_2 + 3BiO(e^-) + 3H^+ \longrightarrow N_2H_3 \quad (2)$$

$$N_2H_3 + 3BiO(e^-) + 5H^+ \longrightarrow 2NH_4^+ \quad (3)$$

$$N_2H_3 + BiO(e^-) + H^+ \longrightarrow N_2H_4 \quad (4)$$

$$2N_2H_3 \longrightarrow 2N_2 + 3H_2 \quad (5)$$

$$3H_2O + 6BiO(h^+) \longrightarrow 3/2O_2 + 6H^+ \quad (6)$$

First, simulated solar light excited electrons and holes were generated on the BiO catalyst (equation 1). Then the photogenerated electrons may transfer to the surface and participate in a one-step three electron N_2 reduction process to obtain N_2H_3

intermediate (equation 2) due to the possible $1N_2$-3Bi side-on bond structure. N_2H_3 intermediate will be further reduced into NH_4^+ (equation 3) or N_2H_4 (equation 4) by a subsequent one step three-electron or one-electron photocatalytic reduction process, respectively. Otherwise, the N_2H_3 intermediate will be decomposed, because it is a short-lived, endothermic compound.[39,40] If the N_2H_3 intermediate is not further reduced, it will decompose into N_2 and H_2 spontaneously (equation 5). In our study, the reaction rates of equations 2, 3 are much higher than that of equation 5, giving the continuous production of NH_4^+ under the acid conditions. The amount of N_2H_4 in the final product was only about 1.6 %, possibly because of the $1N_2$-3Bi side-on coordinating mode of N_2 which facilitate three electron reduction process (equations 2, 3). During the photocatalytic N_2 reduction process, O_2 was produced from water oxidation by photogenerated holes (equation 6). The theoretical molar ratio of the generated NH_4^+ to O_2 from the above equations is 1.33. In a closed reaction system which filled with pure N_2 and water, we observed a continuous O_2 evolution (Fig. S8) along with a prolonged irradiation time and a total amount of 117 μmol O_2 was obtained when generating 2.32 mg NH_4^+. The molar ratio of the generated NH_4^+ to O_2 is 1.41, which is close to the theoretical value. Besides, a tiny amount of H_2 (2.4 μmol) was also detected within 24 h in the closed reaction system, which may be originated from the decomposition of trace amount of unconverted N_2H_3 intermediate.

Conclusions

In summary, bismuth monoxide quantum dots were successfully synthesized by a facile hydrothermal synthesis method using oleate as capping agent. Different from

View Article Online
DOI: 10.1039/C6TA09275F

the other previously reported N_2 reduction photocatalysts which have limited and randomly distributed defect-type N_2 activation centers, the BiO catalyst has all of the lattice bismuth species as potential activation centers. This characteristic makes the as-synthesized BiO a highly efficient photocatalyst for solar N_2 reduction to ammonia. The ammonia synthesis rate is up to 1226 μmol/g·h without the assistant of any sacrificial agent or co-catalyst, which is about 1000 times higher than that of previously reported traditional Fe-TiO_2 photocatalyst. More importantly, the photocatalytic activity does not show any obvious deactivation even after 120 h. Kinetic studies by electrochemical measurements and quantum chemical calculations indicate the highly improved photocatalytic performance of BiO may be ascribed to the cooperation of three low valent surface Bi (II) species for N_2 activation. This study may open up new opportunities for designing highly efficient and robust solar light photocatalyst for artificial ammonia synthesis under ambient conditions.

Acknowledgment

This work was financially supported by the National Basic Research Program of China (2013CB933200), National Natural Science Foundation of China (21671197, 51272269, 51272303, 51472260), and the research grant (16ZR1440800) from Shanghai Science and Technology Commission. Prof. Guangyu Li from Shanghai Institute of Organic Chemistry is gratefully acknowledged for measurement and interpretation of the NMR data.

Supplementary Materials

Figure S1-S8.

References

1. T. Rosswall, in *Some Perspectives of the Major Biogeochemical Cycles* (ed. Likens, G. E.) Ch. 2 (Wiley, New York, 1981).

2. J. B. Howard, D. C. Rees, *Chem. Rev.* 1996, **96,** 2965−2982.

3. B. M. Hoffman, D. R. Dean, L. C. Seefeldt, *Acc. Chem. Res*. 2009, **42**, 609–619.

4. R. Navarro-González, C. P. McKay, D. N. Mvondo, *Nature* 2001, **412**, 61−64.

5. S. Gambarotta, J. Scott, *Angew. Chem. Int. Ed.* 2004, **43**, 5298–5308.

6. A. J. Pool, E. Lobkovsky, P. J. Chirik, *Nature* 2004, **427**, 527–530.

7. V. Smil, *Enriching the Earth: Fritz Haber, Carl Bosch and the Transformation of World Food Production* (MIT Press, Cambridge, MA, 2001).

8 C. Sivasankar, S. Baskaran, M. Tamizmani, K. Ramakrishna, *J. Organomet. Chem.* 2014, **752**, 44–58.

9. R. Schlögl, *Angew. Chem. Int. Ed.* 2003, **42**, 2004–2008.

10. H. Bielawa, O. Hinrichsen, A. Birkner, M. Muhler, *Angew. Chem. Int. Ed*. 1999, **40**, 1061–1063.

11. T. Shima, S. Hu, G. Luo, X. Kang, Y. Luo, Z. Hou, *Science* 2013, **340**, 1549−1552.

12. Y. Tanabe, Y. Nishibayashi, *Coordin. Chem. Rev*. 2013, **257**, 2551–2564.

13. G. N. Schrauzer, T. D. Guth, *J. Am. Chem. Soc.* 1977, **99**, 7189–7193.

14. E. Endoh, J. K. Leland, A. J. Bard, *J. Phys. Chem.* 1986, **90,** 6223−6226.

15. H. Li, J. Shang, Z. Ai, L. Zhang, *J. Am. Chem. Soc.* 2015, **137**, 6393–6399.

16. H. Kisch, *Angew. Chem. Int. Ed*. 2013, **52**, 812–847.

17. V. Augugliaro, A. Lauricella, L. Rizzuti, M. Schiavello, A. Sclafani, *Int. J. Hydrogen Energ.* 1982, **7**, 845−850.

18. J. Soria, J. C. Conesa, V. Augugliaro, L. Palmisano, M. Schiavello, A. Sclafani, *J. Phys. Chem*. 1991, **95**, 274−282.

View Article Online
DOI: 10.1039/C6TA09275F

19. O. P. Linnik, H. Kisch, *Mendeleev Commun*. 2008, **18**, 10–11.

20. L. Palmisano, V. Augugliaro, A. Sclafani, M. Schiavello, *J. Phys. Chem*. 1988, **92**, 6710−6713.

21. K. Tennakone, S. Punchihewa, R. Tantrigoda, *Sol. Energy Mater*. 1989, **18**, 217−221.

22. O. Rusina, A. Eremenko, G. Frank, H. P. Strunk, H. Kisch, *Angew. Chem. Int. Ed*. 2001, **40**, 3993−3995.

23. W. Zhao, J. Zhang, X. Zhu, M. Zhang, J. Tang, M. Tan, Y. Wang, *Appl. Catal. B: Environ*. 2014, **144**, 468–477.

24. G. Dong, W. Hob, C. Wang, *J. Mater. Chem. A* 2015, **3**, 23435–23441.

25. M. Kitano, Y. Inoue, Y. Yamazaki, F. Hayashi, S. Kanbara, S. Matsuishi, T. Yokoyama, S. W. Kim, M. Hara, H. Hosono, *Nature Chem.* 2012, **4**, 934−940.

26. G. Ertl, *Angew. Chem. Int. Ed*. 2008, **47**, 3524–3535.

27. M. M. Rodriguez, E. Bill, W. W. Brennessel, P. L. Holland, *Science* 2011, **334**, 780−783.

28. K. Arashiba, Y. Miyake, Y. Nishibayashi, *Nature Chem.* 2011, **3**, 120−125.

29. B. A. MacKay, M. D. Fryzuk, *Chem. Rev.* 2004, **104**, 385−401.

30. A. Caselli, E. Solari, R. Scopelliti, C. Floriani, N. Re, C. Rizzoli, A. Chiesi-Villa, *J. Am. Chem. Soc.* 2000, **122,** 3652−3670.

31. K. Maeda, T. Takata, M. Hara, N. Saito, Y. Inoue, H. Kobayashi, K. Domen, *J. Am. Chem. Soc.* 2005, **127**, 8286−8287.

32. S. Sun, W. Wang, D. Li, L. Zhang, *ACS Catal.* 2014, **4**, 3498−3503.

33. J. Medina-Ramos, J. L. DiMeglio, J. Rosenthal, *J. Am. Chem. Soc.* 2014, **136**, 8361−8367.

34. L. Liang, F. C. Lei, S. Gao, Y. F. Sun, X. C. Jiao, J. Wu, S. Qamar, Y. Xie, *Angew.*

View Article Online
DOI: 10.1039/C6TA09275F

Chem. Int. Ed. 2015, **54**, 13971−13974.

35. E. Laviron, *J. Electroanal. Chem. Interfacial Electrochem*. 1974, **52**, 355-393.

36. L. Pospíšil, J. Bulíčková, M. Hromadová, M. Gál, S. Civiš, J. Cihelka, J. Tarábek, *Chem. Commun.* 2007, 2270–2272.

37. A. Watanabe, H. Kozuka, *J. Phys. Chem. B* 2003, **107**, 12713−12720.

38. Y. Matsumoto, *J. Solid State Chem*. 1996, **126**, 227−234.

39. N. Bauer, *J. Phys. Chem.* 1960, **64**, 833–837.

40. B. Ruscic, J. Berkowitz, *J. Chem. Phys*. 1991, **95**, 4378−4384.

View Article Online
DOI: 10.1039/C6TA09275F

Figure captions

Fig. 1 Schematic illustration of the whole synthesis procedure for the BiO quantum dots.

Fig. 2 Characterizations for the hydrothermally synthesized BiO sample. a. Low magnified TEM image of the BiO sample. b, High magnified TEM image. c, High resolution TEM image. d, The related schematic atomic model of BiO, clearly showing atomic configuration of Bi/O and hexagonal tunnel structure along the [010] direction. e, XRD pattern of the as-prepared BiO sample. f, XPS spectrum of the as-prepared BiO sample in the Bi $4f_{5/2}$ and Bi $4f_{7/2}$ binding energy region.

Fig. 3 Photocatalytic N_2 reduction performance of the as-prepared BiO sample at different conditions under simulated solar light irradiation. a, The generated ammonia concentrations at different irradiation time in pure water, inset: the corresponding ammonia synthesis rate. b, The generated ammonia concentrations at different irradiation time in 15 vol% methanol solution. c, Photostability of the as-prepared BiO sample for N_2 reduction under simulated solar light at acid conditions (pH3.8). d, Comparison of experimental infrared spectra of NH_4^+ obtained after N_2 photoreduction on BiO catalyst using 50% $^{15}N_2$ labelled N_2 and pure $^{14}N_2$ respectively.

Fig. 4 Quantum chemical calculations of N_2 activation and hydrogenation performance of BiO catalyst based on density functional theory. (a, b) The calculated charge density plot at valence band maximum (VBM) of BiO {010} surfaces, a: top view, b: side view. The yellow and blue isosurfaces represent charge accumulation and depletion in the space, respectively. c, The N-N bond distance evolutions with adding hydrogen atoms on BiO {010} surface. d, The binding energy of N_2H_n on BiO {010} surface.

View Article Online
DOI: 10.1039/C6TA09275F

Fig. 5 Kinetic study of N_2 reduction on BiO catalyst by electrochemical measurements in N_2 saturated 0.5 M Na_2SO_4 under room temperature (25 ℃) and simulated solar light irradiation. a, Cyclic voltammograms of BiO electrode at pH=3.8. b, Cyclic voltammograms of BiO electrode at pH=7. Inset: the plot for the reduction peak potential (Ep) vs. lnν (scan rate). c, Cathodic electrochemical scans on the as-prepared BiO electrode under chopped simulated solar light irradiation. d, Mott−Schottky plot of the as-prepared BiO electrode in 0.5 M Na_2SO_4 at pH=7.

Fig. 6 Possible pathway for N_2 activation and hydrogenation on BiO catalyst. a, Schematic electron donation from the lone pairs of three Bi atoms to the three unoccupied anti-bonding orbitals (σ^*2p_x, π^*2p_y, and π^*2p_z) of N_2 molecular, forming a $1N_2$-3Bi(II) side-on bound structure. b, The whole N_2 activation and reduction process on BiO catalyst.

View Article Online
DOI: 10.1039/C6TA09275F

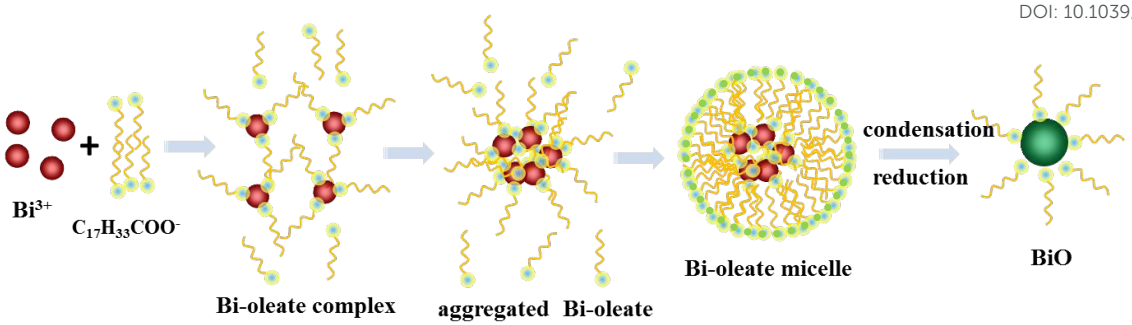

Fig. 1

View Article Online
DOI: 10.1039/C6TA09275F

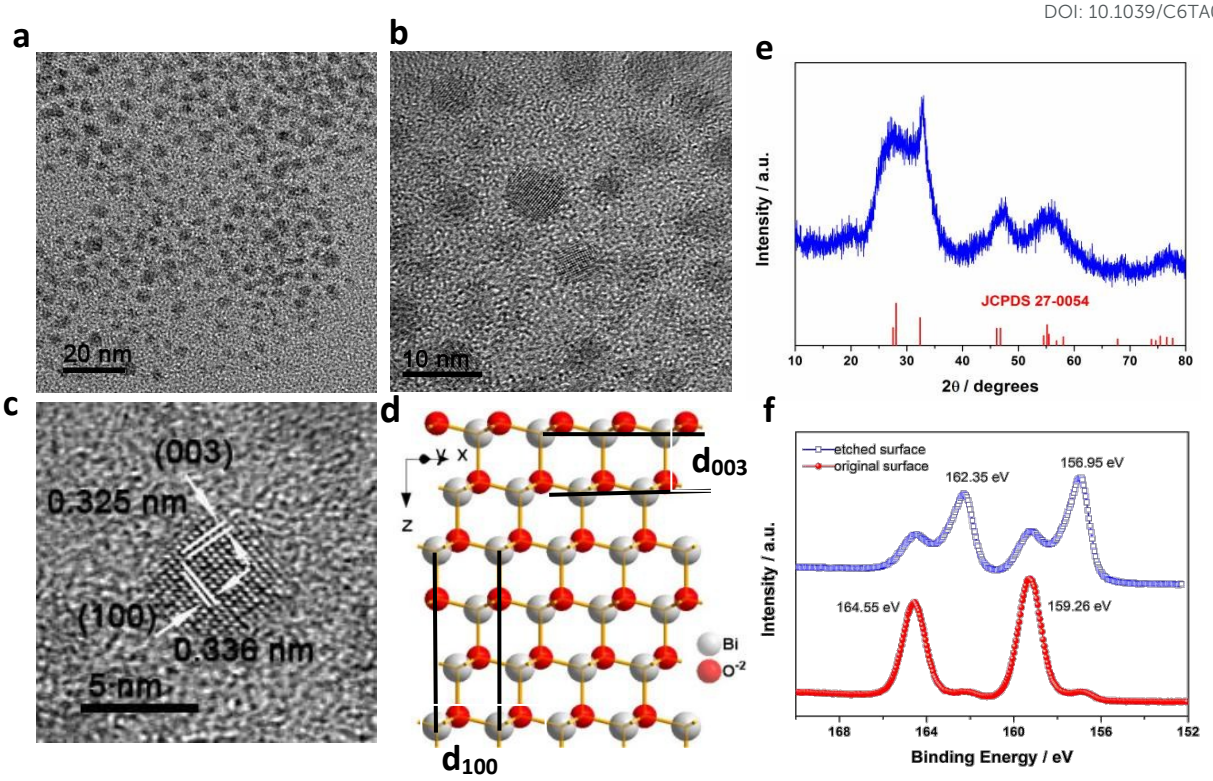

Fig. 2

View Article Online
DOI: 10.1039/C6TA09275F

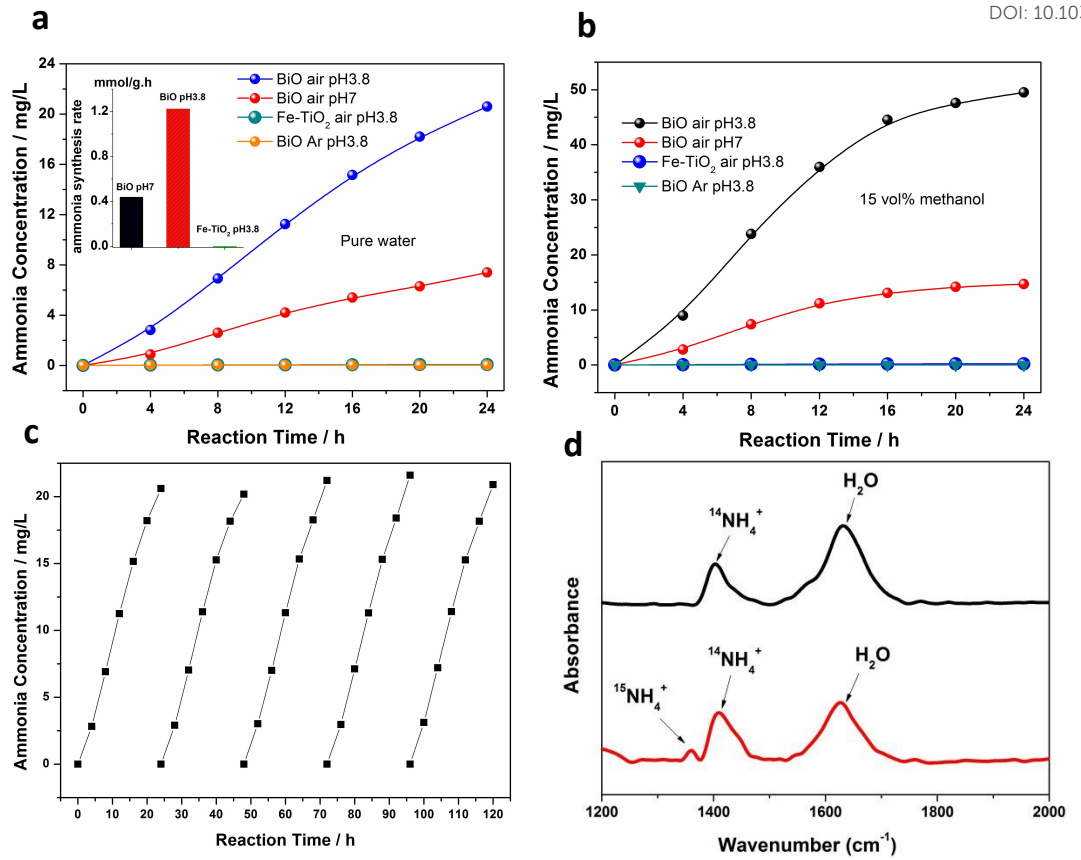

Fig. 3

View Article Online
DOI: 10.1039/C6TA09275F

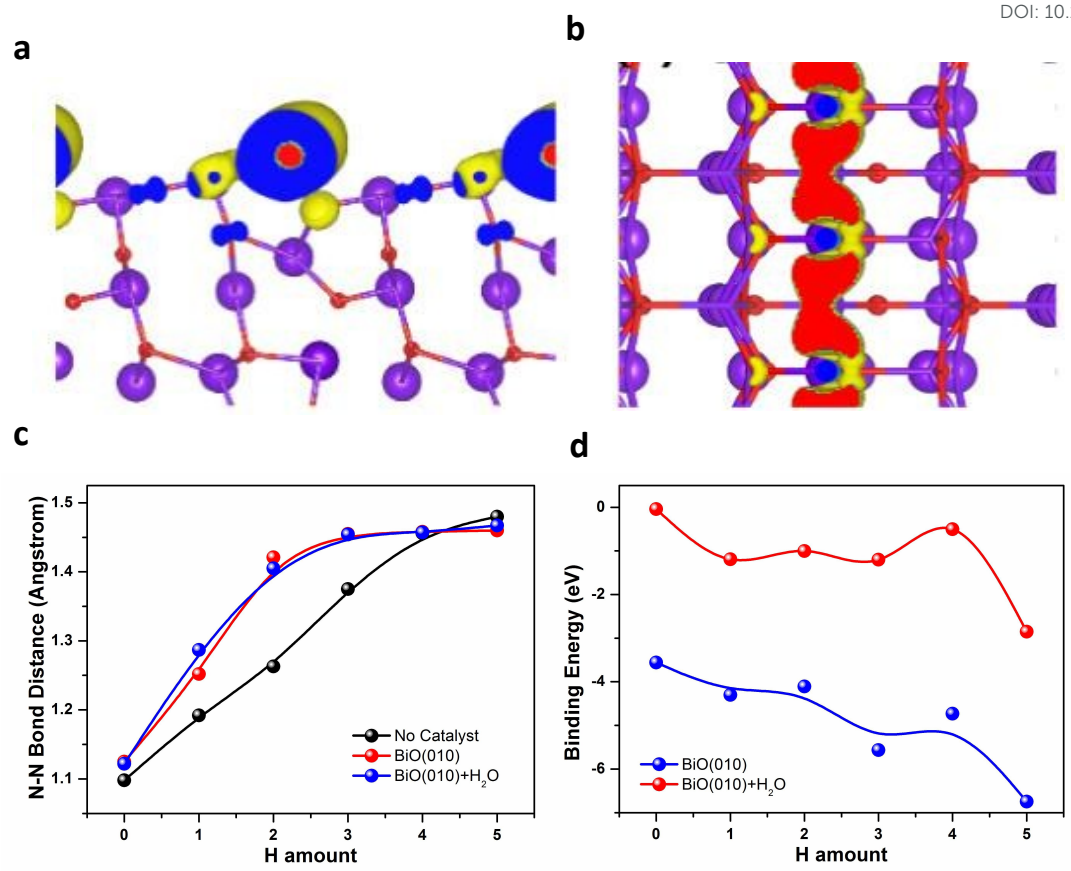

Fig. 4

View Article Online
DOI: 10.1039/C6TA09275F

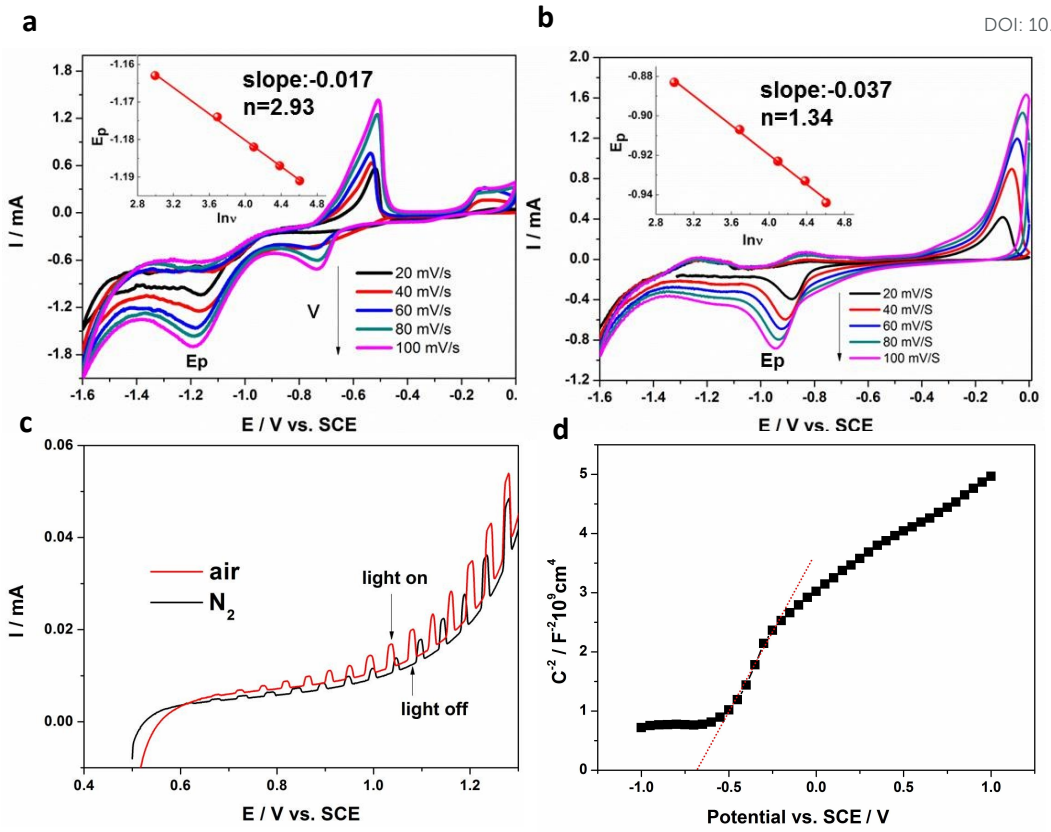

Fig. 5

View Article Online
DOI: 10.1039/C6TA09275F

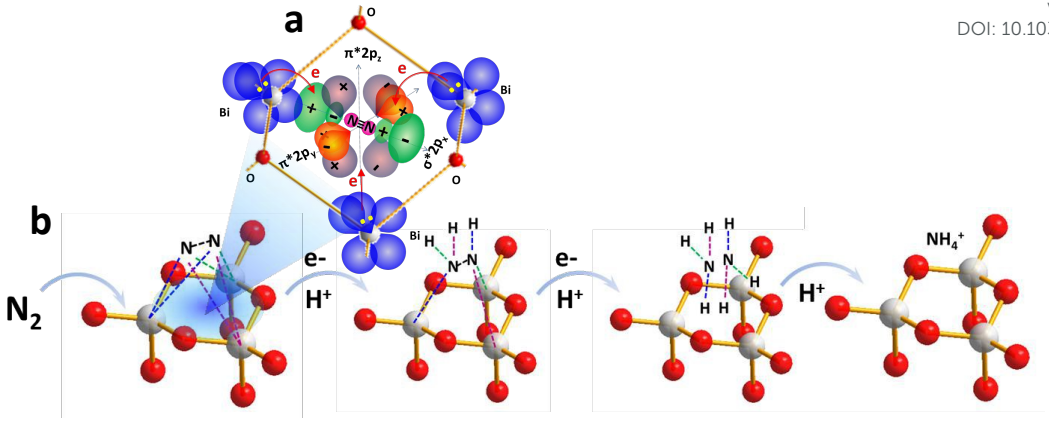

Fig. 6

Table of contents

View Article Online
DOI: 10.1039/C6TA09275F

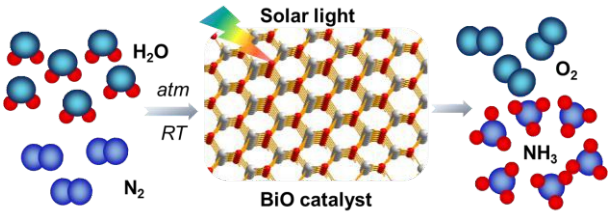

An efficient and sustainable production of ammonia from water and air under simulated solar light is achieved by BiO photocatalyst.